Ionics (2020) 26:3387–3394
https://doi.org/10.1007/s11581-020-03468-x

ORIGINAL PAPER

Crystal doping of K ion on Na site raises the electrochemical performance of $NaTi_2(PO_4)_3$/C anode for sodium-ion battery

Na Liu[1] · Zhangxing He[1,2] · Jing Zhu[1] · Lei Dai[1,2] · Yuehua Li[1] · Wei Meng[1] · Ling Wang[1,2]

Received: 5 November 2019 / Revised: 14 January 2020 / Accepted: 19 January 2020 / Published online: 28 January 2020

Abstract

Sodium-ion battery is a rocking chair battery similar to lithium-ion battery and is considered to have a promising future due to low cost and extensive resources. As anode for sodium-ion battery, $NaTi_2(PO_4)_3$ has attracted lots of attention due to its thermal stability and three-dimensional channels. In this work, we employed crystal doping of K ion on Na site to raise electrochemical performance of $NaTi_2(PO_4)_3$/C composites. $NaTi_2(PO_4)_3$/C doped with K was synthesized and used as anode for sodium-ion battery. XRD and SEM results imply that introduction of K ion has no significant change in the main crystal form and morphology of materials. Among $Na_{1-x}K_xTi_2(PO_4)_3$/C ($x = 0$, 0.01, 0.03, 0.05) composites, $Na_{0.97}K_{0.03}Ti_2(PO_4)_3$/C (NC/K-3) shows the best rate property, outstanding cycling performance, and the lowest charge transfer resistance. It delivers capacities of 206.65, 139.14, and 94.45 mAh g^{-1} at 0.1, 1.2, and 3 A g^{-1}, severally. Besides, even after 1000 cycles at 1.2 A g^{-1}, NC/K-3 keeps the discharge capacity at 89.5 mAh g^{-1} and 39.2 mAh g^{-1} higher than that of bare $NaTi_2(PO_4)_3$/C. In conclusion, K doping on Na site by sol-gel route is a viable modification method to improve performance of $NaTi_2(PO_4)_3$/C composite as anode for sodium-ion batteries.

Keywords $NaTi_2(PO_4)_3$ · NASICON structure · Cation doping · Anode · Sodium ion batteries

Introduction

Fossil fuels bring a range of environmental pollution problems, and more and more new energy sources are being used in response to sustainable development requirements [1–5]. Wind and solar energy is limited by time and location and requires continuous and efficient energy storage systems to provide a sustainable energy supply [6–9]. Secondary electrochemical battery is a pivotal technology for large-sized energy storage systems [10–13]. Among them, lithium-ion batteries are suitable for a variety of electronic devices and large-sized energy storage, such as smart phones, electric bicycles, and so on [14–18]. In addition, the demand of power storage systems such as electric vehicles and hybrid vehicles is also increasing [19, 20]. Lithium resources are being consumed more and more, leading to its high price and resource lack [21, 22]. Therefore, it makes sense to research and develop other new battery systems [23].

Sodium-ion batteries are expected to buffer excessive demand for lithium-ion batteries [24–26], which have attracted widespread attention from battery researchers. The cost of sodium-ion batteries is low due to abundant sodium reserves and wide range of sources [27]. Low-cost batteries also contribute to the further application and development of energy storage systems [28]. As a result, reports on sodium-ion batteries have increased incredibly in last decades [29, 30]. Many electrode materials have been studied, such as carbon materials [31, 32], TiO_2 [33], SnS_2 [34], $Na_2Ti_3O_7$ [35], $NaVO_2$ [36], $LiTi_2(PO_4)_3$ [37], and $NaTi_2(PO_4)_3$ [38] as anode materials and Na_xMnO_2 [39], Na_xCoO_2 [40], $Na_3V_2(PO_4)_3$ [41], and $NaFePO_4$ [42] as cathode materials. The working process of sodium-ion batteries is realized by transfer of electrons and

✉ Zhangxing He
zxhe@ncst.edu.cn

✉ Lei Dai
dailei_b@163.com

✉ Ling Wang
tswling@126.com

[1] School of Chemical Engineering, North China University of Science and Technology, Tangshan 063009, China

[2] Hebei Province Key Laboratory of Photocatalytic and Electrocatalytic Materials for Environment, North China University of Science and Technology, Tangshan 063009, China

the intercalation/deintercalation of sodium ions. They are "rocking chair type" batteries [43, 44] like lithium-ion batteries. But in terms of ionic radius, Na is larger than Li, which tends to cause greater expansion in volume during insertion process, further resulting in unsatisfactory cycling stability and inferior specific capacity [45]. Hence, to meet increasing demand, the development of suitable electrode materials for sodium storage remains a huge challenge.

$NaTi_2(PO_4)_3$ possesses Na superionic conductor (NASICON) structure and is a class of fast ion conductor material [46, 47]. The [TiO_6] octahedron and [PO_4] tetrahedron in the $NaTi_2(PO_4)_3$ crystal are interconnected by oxygen atoms at the apex to form a $[Ti_2(PO_4)_3]^-$ polyanion structure [48, 49]. It has large channels inside, which are very suitable for the rapid transmission of lithium ions and sodium ions. However, its intrinsic conductivity is low, and this shortcoming is usually improved by combining with conductive additives or carbon [50, 51]. For instance, Zuo et al. [52] have proposed and manufactured reduced graphene and carbon co-modified $NaTi_2(PO_4)_3$ sample by hydrothermal process and high-temperature calcination. Graphene and coated carbon can form a conductive network in this composite, which effectively improves the conductivity and sodium storage performance. At 0.1 C, the corresponding discharge capacity of modified $NaTi_2(PO_4)_3$ can reach 129 mAh g^{-1}. Another way to improve conductivity is ion doping [53], including anion doping and cation doping. Su et al. [54] have proposed a novel nanostructured $Na_{1-2x}Ti_2(PO_4)_{3-x}F_x$ anode for sodium-ion batteries. Appropriate fluorine doping increases the ion/electron transport speed, resulting in ultralong cycle life. Capacity decay of $Na_{2.9}Ti_2(PO_4)_{2.95}F_{0.05}$/C at 10 °C is only 10% after 1000 cycles.

In this paper, crystal doping strategy was employed to raise the sodium storage performance of $NaTi_2(PO_4)_3$/C compounds for sodium-ion battery. We used potassium instead of sodium partially and phenolic resin as carbon resource to construct $Na_{1-x}K_xTi_2(PO_4)_3$/C anode materials. An easy sol-gel approach was utilized to prepare composites, roughly as depicted in Fig. 1. And the electrochemical behavior of all samples is reported in this paper.

Experimental

Synthesis

$Na_{1-x}K_xTi_2(PO_4)_3$/C ($x = 0, 0.01, 0.03, 0.05$) compounds were designed and compounded as following the steps. By stirring to form initial solution, 1.7202 g $Ti(OC_4H_9)_4$ and 15 mL ethanol were mixed. H_3PO_4, $CH_3COONa{\cdot}3H_2O$, and CH_3COOK with stoichiometric ratio were added to the solution. After that, 2-mL concentrated hydrochloric acid and 0.17-g phenolic resin were added successively and then stirred for 3 h at 55 °C in closed condition and dried for 10 h at 80 °C in open condition. Each precursor was calcined for 5 h at 750 °C in argon-filled tube furnace. $Na_{1-x}K_xTi_2(PO_4)_3$/C ($x = 0, 0.01, 0.03, 0.05$) compounds were abbreviated as NC, NC/K-1, NC/K-3, and NC/K-5, respectively.

Characterizations

Crystal type of four samples were examined by X-ray diffraction (XRD), conducted on X-ray diffractometer (D/MAX2500PC) with the radiation of Cu-Kα. Morphology features of as-prepared samples and electrodes after cycling testing were investigated through S-4800 scanning electron microscopy (SEM) manufactured in Hitachi. Each cycled electrode was obtained by disassembling the cell. And the electrode was rinsed by absolute ethanol a few times. Then it was dried for 8 h at 80 °C.

Electrochemical measurements

Composite powder, polyvinylidene fluoride (PVDF), and super P were blended based on a mass ratio of 7:1.5:1.5 and then dissolved in N-methyl-2-pyrrolidone (NMP). The liquid mixture was coated on Cu foil. After drying for 6 h at 80 °C, working electrode was got after cutting Cu foil into small wafer with diameter of 14 mm. The mass load of electrode was 1.5–2.0 mg cm^{-2}. CR2016 half cell used metallic sodium as counter electrode, glass fiber as membrane, and prepared electrode as working electrode. Electrolyte was 1 M $NaClO_4$ dissolved in mixed organic solvents, including DMC, EC, and

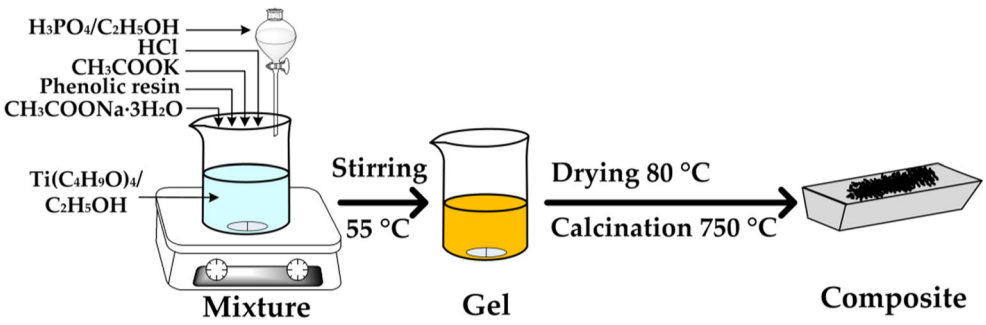

Fig. 1 Schematic diagram of the synthesis process of $Na_{1-x}K_xTi_2(PO_4)_3$/C composites

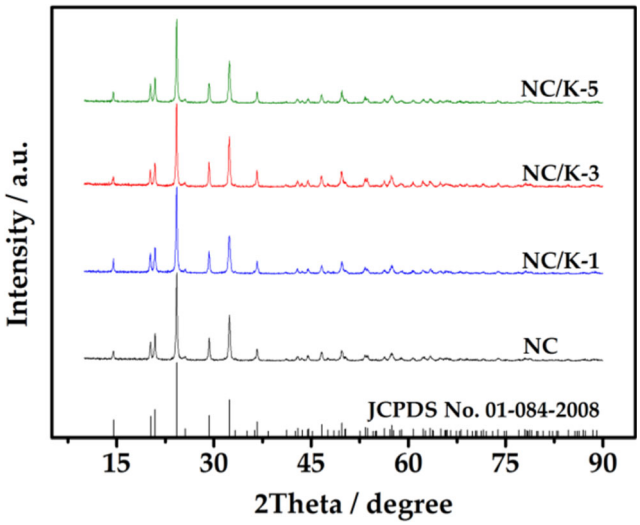

Fig. 2 XRD patterns of all samples

EMC with volume ratio of 1:1:1. In addition, 5% FEC was added to the electrolyte to make it more stable. All cells were assembled in the glove box with oxygen and water < 0.1 ppm. Chenhua electrochemical workstation (CHI660E) was employed to conduct electrochemical impedance spectroscopy (EIS) and cyclic voltammetry (CV) tests for cells. The scan rate and voltage window for CV tests were 0.2 mV s^{-1} and 0.01–3 V, respectively. The frequency and amplitude for EIS tests were 0.01–100,000 Hz and 5 mV, severally. EIS tests for cells were performed after activating at 0.04 A g^{-1} for 5 cycles and then charging to 2.1 V for 2 h. Rate and cycling performance were conducted on Neware battery testing system (CT-3008W), which were tested by galvanostatic charge-discharge mode. The rates for rate performance varied from 0.04 to 3 A g^{-1}. Cycling performance was tested at current of 1.2 A g^{-1} for 1000 cycles.

Results and discussion

Figure 2 displays XRD pattern of all samples. Clear diffraction peaks reflect crystal form characteristics of NASICON-type $NaTi_2(PO_4)_3$. Four sets of similar diffraction peaks indicate similar crystal structure of four samples, all of which are ascribed to the rhombohedral structure of $NaTi_2(PO_4)_3$ (JCPDS No. 01–084-2008). The obvious diffraction peaks of impurity do not appear, indicating that each synthesized complex has the pure phase.

As seen in Fig. 3, SEM images exhibit the surface morphology comparison of NC and NC/K-3. It can be seen that the overall morphology of two materials is loose, with some agglomeration. As shown in high-magnification images, nano-sized particles exist in both materials. Small nanoparticles and loose structure can help the transport of Na ions between electrolyte and crystal. Pristine and K-doped $NaTi_2(PO_4)_3$ demonstrate no obvious difference on the dispersion and particle size. It shows that the doping of K ion on Na site does not have a momentous influence on morphology of composite. Good stability of morphology is beneficial to get the reason of improved performance of K-doped sample.

Cyclic voltammetry tests of NC and NC/K-3 were conducted on half cells, and cyclic voltammetry curves are shown in Fig. 4. Two sharp redox peaks indicate that both NC and NC/

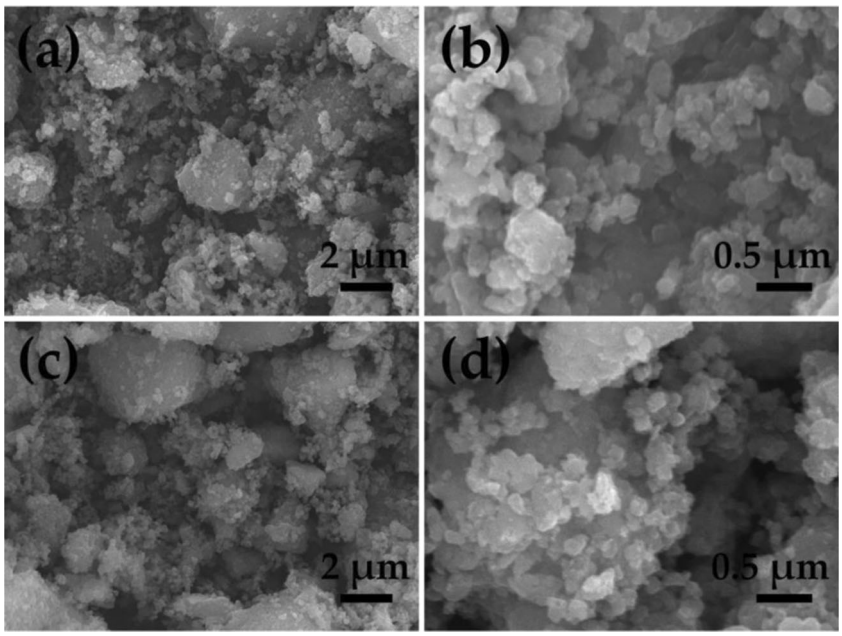

Fig. 3 SEM images for NC (**a**, **b**) and NC/K-3 (**c**, **d**) at different magnifications

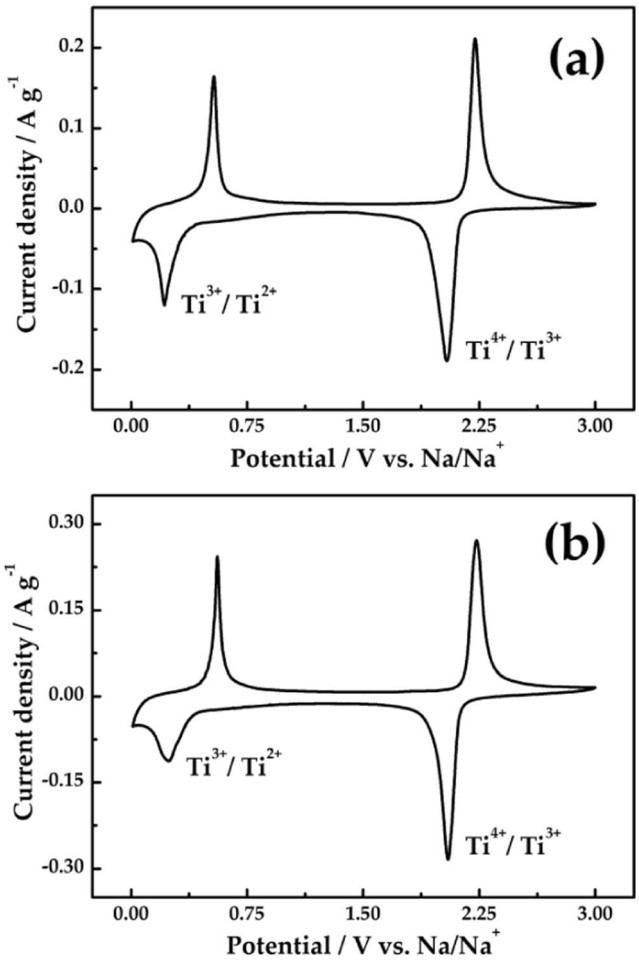

Fig. 4 Cyclic voltammetry curves of NC (**a**) and NC/K-3 (**b**) composites at scan rate of 0.2 mV s^{-1}

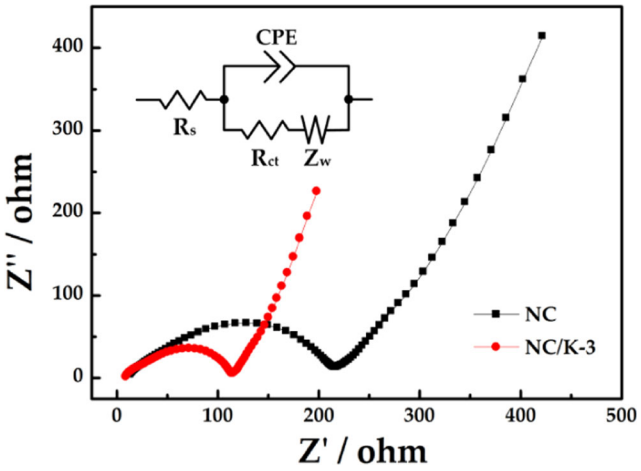

Fig. 5 Electrochemical impedance spectra for NC and NC/K-3

K-3 electrodes can realize the reversible intercalation/deintercalation of sodium ions. The peaks located at 1.89–2.35 V and 0.13–0.61 V correspond to redox reactions of Ti^{4+}/Ti^{3+} and Ti^{3+}/Ti^{2+}, respectively. From Fig. 4a, oxidation and reduction peak current densities at about 2.1 V for NC are 0.21 and 0.19 A g^{-1}, severally. And those for NC/K-3 are 0.29 and 0.28 A g^{-1} (Fig. 4b). Peak current densities increase obviously for NC/K-3, demonstrating that the K-doping strategy is effective. Furthermore, peak current densities at around 0.4 V for NC/K-3 are also higher than those of NC. Cyclic voltammetry data illustrate that sodium storage properties of NC/K-3 are better than those of NC coming from the efficient crystal doping, as K doping cannot affect the morphology of composites, which is confirmed by the SEM results.

Aiming at discussing the kinetic process of charge transfer in electrode, EIS tests are carried out on half cells, and spectra are displayed in Fig. 5. As seen from Nyquist plot, the low-frequency line means Warburg impedance (Z_w), and middle-frequency semicircle means charge transfer resistance (R_{ct}). The larger slope of line for NC/K-3 indicates that sodium ions diffuse faster in the NC/K-3 electrode than NC electrode [55]. It is noted that R_{ct} for NC and NC/K-3 are 201.31 Ω and 106.27 Ω, severally. The smaller R_{ct} data illustrate that NC/K-3 electrode has a faster intercalation/deintercalation kinetics of sodium ions. This may be due to the increase in unit cell volume of NC/K-3 after K doping, which provides a wider intercalation/deintercalation channel for sodium ions and accelerates the migration of sodium ions [56]. At high frequency, two curves both have an intercept on Z-axis, corresponding to ohmic resistance (R_s). Two composites exhibit the similar R_s, which implies that K doping has no obvious effect on electrical conductivity.

The rate performances of four samples are given in Fig. 6. Three samples with K doping have a significant increase in discharge capacity, and NC/K-3 reaches the highest discharge capacity in four samples. NC/K-3 delivers discharge capacities of 206.65, 139.14, and 94.45 mAh g^{-1} at 0.1, 1.2, and 3 A g^{-1}, severally, which are 118.54, 100.09, and 69.53 mAh g^{-1} higher when compared with the bare NC. When current density goes from 3 to 0.1 A g^{-1}, NC/K-3 can keep discharge capacity at 197.75 mAh g^{-1}. This value almost reaches 95.8% of its original value, indicating excellent reversibility of NC/K-3 electrode. The improved properties of K-doped composite are probably attributed to that K doping can lead to the increase in unit cell volume. This can also be seen in previous reports. Xia et al. [57] prepared K-doped $Na_3Fe_2(PO_4)_3$ cathode materials for sodium-ion battery and found lattice parameters indeed increase after K doping. The unit cell volume of K-doped samples increases slightly compared with blank $Na_3Fe_2(PO_4)_3$. Excessive doping may cause slight damage to the lattice structure, resulting in poor electrochemical performance. Charge-discharge profiles at different current densities for NC and NC/K-3 are given in Fig. 6b and c. All profiles exhibit planus plateaus for charging and discharging at 2.1 and

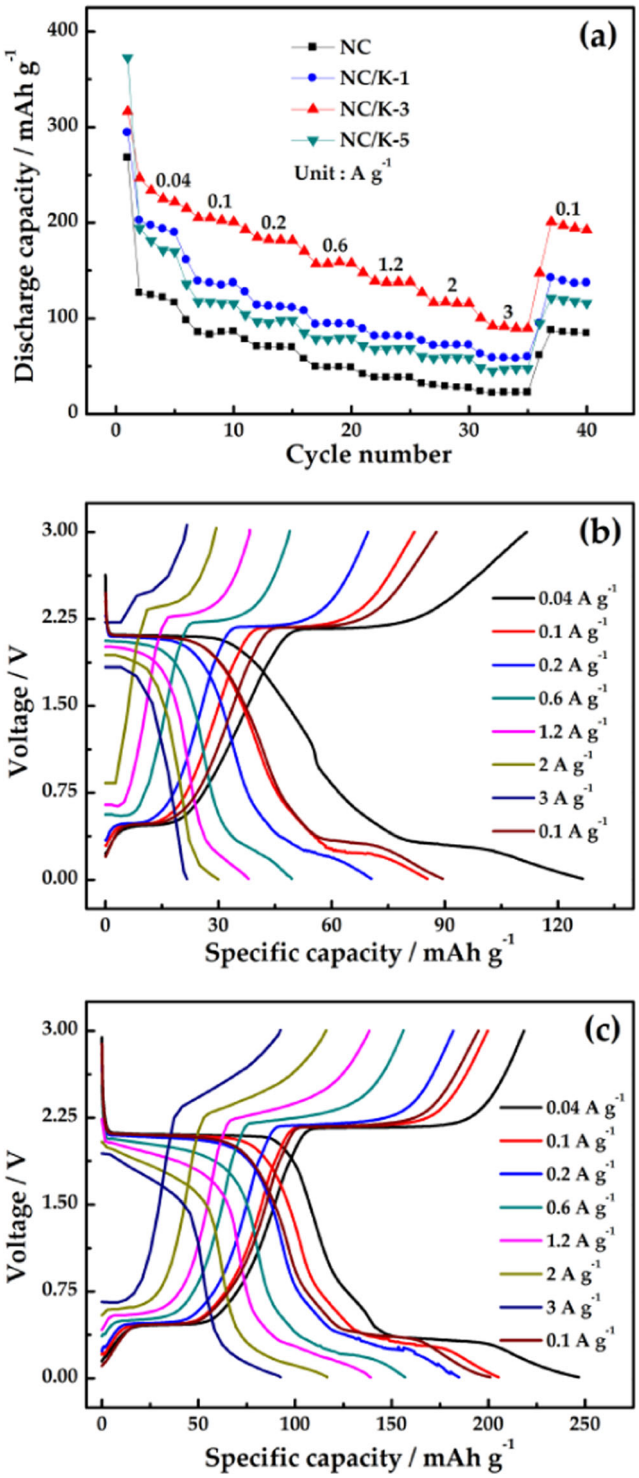

Fig. 6 Rate performance of four samples (**a**), charge-discharge profiles for NC (**b**), and NC/K-3 (**c**) at different rate

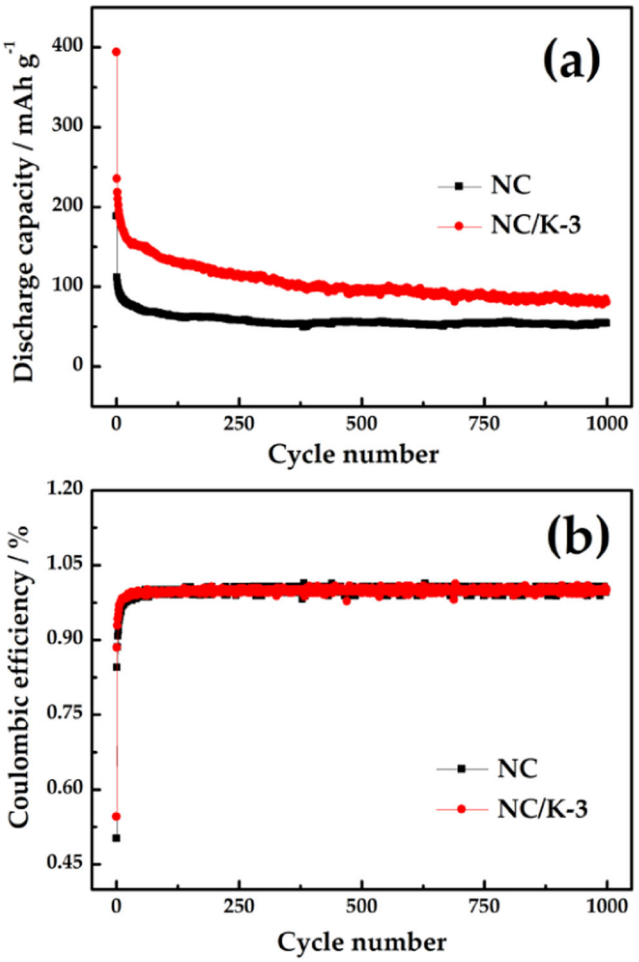

Fig. 7 Cycling performance (**a**) and coulombic efficiency (**b**) for NC and NC/K-3 at 1.2 A g^{-1}

0.4 V approximately, which correspond with two pairs of redox peaks in CV tests. All plateaus for NC/K-3 are longer and more stable, and this advantage is more pronounced for plateaus around 0.4 V. With the increase of current, the stable existence of the charging and discharging plateaus indicates good rate performance for NC/K-3.

Figure 7 displays long-term cycling performance of two samples and coulombic efficiency for each cycle. The initial discharge capacity and coulomb efficiency of NC/K-3 are higher than those of NC. Moreover, after charge-discharge process for 1000 cycles, NC/K-3 delivers discharge capacity of 89.5 mAh g^{-1}. In contrast, NC releases lower discharge capacity with value of 50.3 mAh g^{-1}. Discharge capacities of NC/K-3 are always higher than those of NC. Apparently, NC/K-3 demonstrates excellent cycling performance at high current density. This is in accord with the rate results. From Fig. 7b, coulombic efficiency for NC and NC/K-3 is about 100% after increasing in first few cycles, implying stable and high-efficient nature of cells.

In order to investigate the structure stability of NC/K-3, we compared the morphology of NC/K-3 after 100 and 1000 cycles at 1.2 A g^{-1}. SEM images of NC/K-3 after different cycles are shown in Fig. 8. As can be seen from Fig. 8, there is no significant etching and structural comminution on the

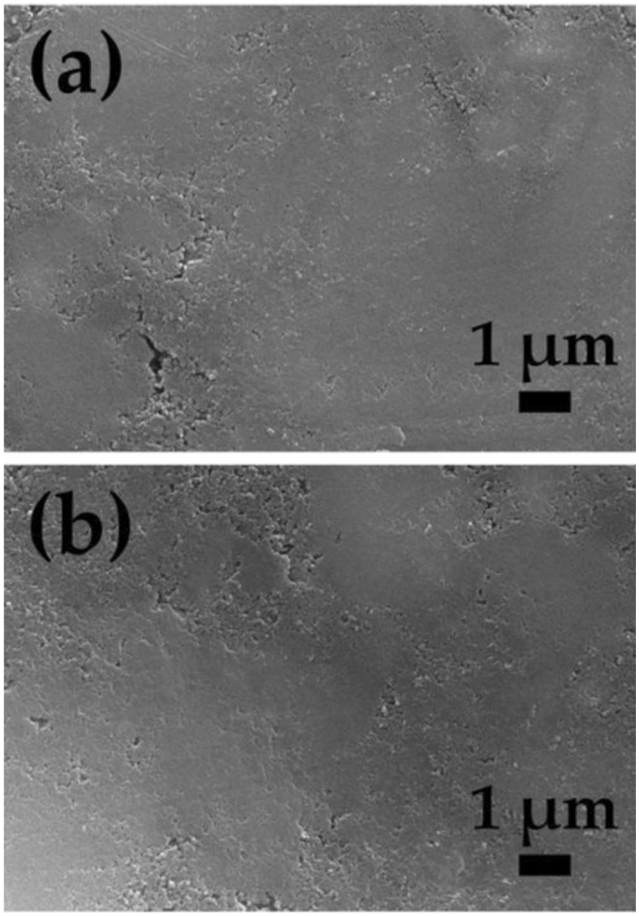

Fig. 8 SEM images of NC/K-3 after 100 (**a**) and 1000 (**b**) cycles at 1.2 A g^{-1}

electrode surface. The stable structure helps to output stable capacity. This also explains the outstanding cycle performance of NC/K-3.

Conclusion

$Na_{1-x}K_xTi_2(PO_4)_3$/C ($x = 0, 0.01, 0.03, 0.05$) compounds were synthesized by simple sol-gel way. A small amount of doped K does not change crystal form of NASICON $NaTi_2(PO_4)_3$ and surface morphology of composites. However, doping of K on Na site for $NaTi_2(PO_4)_3$ has obvious effect on its electrochemical performance and has been shown to be positive. NC/K-3 delivers the highest discharge capacity at different rates in four composites (206.65, 139.14, and 94.45 mAh g^{-1} at 0.1, 1.2, and 3 A g^{-1}). As comparison, NC delivers 88.11, 39.05, and 24.92 mAh g^{-1} at 0.1, 1.2, and 3 A g^{-1}, severally. Moreover, NC/K-3 also has long cycling life and high capacity (89.5 mAh g^{-1} after 1000 cycles at 1.2 A g^{-1}). These elementary electrochemical data imply that K-doped $NaTi_2(PO_4)_3$ is a potential competitive anode material in sodium-ion battery.

Funding information This work was financially supported by National Natural Science Foundation of China (No. 51504079), Hebei Natural Science Fund for Distinguished Young Scholar of China (No. E2019209433).

References

1. Qi S, Xu B, Tiong VT, Hu J, Ma J (2020) Progress on iron oxides and chalcogenides as anodes for sodium-ion batteries. Chem Eng J 379:122261–122292
2. He X, Sun Z, Zou Q, Wu L, Jiang J (2019) Electrochemical behavior of Co(II) reduction for preparing nanocrystalline Co catalyst for hydrogen evolution reaction from 1-ethyl-3-methylimidazolium bisulfate and ethylene glycol system. J Electrochem Soc 166:D57–D64
3. He X, Sun Z, Zou Q, Yang J, Wu L (2019) Codeposition of nanocrystalline Co-Ni catalyst based on 1-ethyl-3-methylimidazolium bisulfate and ethylene glycol system for hydrogen evolution reaction. J Electrochem Soc 166:D908–D915
4. Jiang Y, Feng X, Cheng G, Li Y, Li C, He Z, Zhu J, Meng W, Zhou H, Dai L, Wang L (2019) Electrocatalytic activity of MnO_2 nanosheet array-decorated carbon paper as superior negative electrode for vanadium redox flow batteries. Electrochim Acta 322:134754–134762
5. Li C, Wang M, Xie B, Ma H, Chen J (2020) Enhanced properties of diatomite-based composite phase change materials for thermal energy storage. Renew Energy 147:265–274
6. Liu Y, Qiao Y, Zhang W, Li Z, Ji X, Miao L, Yuan L, Hu X, Huang Y (2015) Sodium storage in Na-rich $Na_xFeFe(CN)_6$ nanocubes. Nano Energy 12:386–393
7. He Z, Cheng G, Jiang Y, Li Y, Zhu J, Meng W, Zhou H, Dai L, Wang L (2020) Novel 2D porous carbon nanosheet derived from biomass: Ultrahigh porosity and excellent performances toward V^{2+}/V^{3+} redox reaction for vanadium redox flow battery. Int J Hydrogen Energy 45:3959–3970
8. Jiang Z, Li Y, Zhu J, Li B, Li C, Wang L, Meng W, He Z, Dai L (2019) Synthesis and performance of a graphene decorated $NaTi_2(PO_4)_3$/C anode for aqueous lithium-ion batteries. J Alloys Compd 791:176–183
9. Li C, Xie B, He Z, Chen J, Long Y (2019) 3D structure fungi-derived carbon stabilized stearic acid as a composite phase change material for thermal energy storage. Renew Energy 140:862–873
10. Jiang Z, Li Y, Han C, Wu X, He Z, Zhu J, Meng W, Dai L, Wang L (2020) Encapsulation of N-doped carbon layer via in situ dopamine polymerization endows nanostructured $NaTi_2(PO_4)_3$ with superior lithium storage performance. Ceram Int 46:4402–4409
11. Xu B, Qi S, Jin M, Cai X, Lai L, Sun Z, Han X, Lin Z, Shao H, Peng P, Xiang Z, ten Elshof JE, Tan R, Liu C, Zhang Z, Duan X, Ma J (2019) 2020 roadmap on two-dimensional materials for energy storage and conversion. Chin Chem Lett 30:2053–2064
12. Jiang Z, Li Y, Han C, He Z, Ma W, Meng W, Jiang Y, Dai L, Wang L (2020) Superior lithium storage performance of hierarchical N-doped carbon encapsulated $NaTi_2(PO_4)_3$ microflower. Ceram Int 46:1954–1961
13. Fang G, Wang Q, Zhou J, Lei Y, Chen Z, Wang Z, Pan A, Liang S (2019) Metal organic framework-templated synthesis of bimetallic selenides with rich phase boundaries for sodium-ion storage and oxygen evolution reaction. ACS Nano 13:5635–5645
14. Su M, Liu S, Wan H, Dou A, Liu K, Liu Y (2018) Effect of binders on performance of Si/C composite as anode for Li-ion batteries. Ionics 25:2103–2109
15. Wu D, Wang C, Wu M, Chao Y, He P, Ma J (2020) Porous bowl-shaped VS_2 nanosheets/graphene composite for high-rate lithium-ion storage. J Energy Chem 43:24–32

16. Shi M, Kong L, Liu J, Yan K, Li J, Dai Y, Luo Y, Kang L (2015) A novel carbon source coated on C-LiFePO$_4$ as a cathode material for lithium-ion batteries. Ionics 22:185–192
17. Rui X, Sun W, Wu C, Yu Y, Yan Q (2015) An advanced sodium-ion battery composed of carbon coated $Na_3V_2(PO_4)_3$ in a porous graphene network. Adv Mater 27:6670–6676
18. Fang R, Miao C, Mou H, Xiao W (2020) Facile synthesis of Si@TiO$_2$@rGO composite with sandwich-like nanostructure as superior performance anodes for lithium ion batteries. J Alloys Compd 818:152884–152891
19. Sagane F (2016) Synthesis of $NaTi_2(PO_4)_3$ thin-film electrodes by sol-gel method and study on the kinetic behavior of Na^+-ion insertion/extraction reaction in aqueous solution. J Electrochem Soc 163:A2835–A2839
20. Tarascon JM (2010) Is lithium the new gold? Nat Chem 2:510–510
21. Wu M, Xu B, Zhang Y, Qi S, Ni W, Hu J, Ma J (2020) Perspectives in emerging bismuth electrochemistry. Chem Eng J 381:122558–122574
22. Li C, Shi X, Liang S, Ma X, Han M, Wu X, Zhou J (2020) Spatially homogeneous copper foam as surface dendrite-free host for zinc metal anode. Chem Eng J 379:122248–122256
23. Zhao M, Zheng Q, Wang F, Dai W, Song X (2011) Electrochemical performance of high specific capacity of lithium-ion cell LiV_3O_8// $LiMn_2O_4$ with $LiNO_3$ aqueous solution electrolyte. Electrochim Acta 56:3781–3784
24. Chen Z, Zhu D, Li J, Liang D, Liu M, Hu Z, Li X, Feng Z, Huang J (2019) Porous functionalized carbon as anode for a long cycling of sodium-ion batteries. Ionics 25:4517–4522
25. Han MH, Gonzalo E, Singh G, Rojo T (2015) A comprehensive review of sodium layered oxides: powerful cathodes for Na-ion batteries. Energy Environ Sci 8:81–102
26. Fang C, Huang Y, Zhang W, Han J, Deng Z, Cao Y, Yang H (2016) Routes to high energy cathodes of sodium-ion batteries. Adv Energy Mater 6:1501727–1501744
27. Su N, Noor S, Roslee M, Mohamed N, Ahmad A, Yahya M (2018) Potential complexes of $NaCF_3SO_3$-tetraethylene dimethyl glycol ether (tetraglyme)-based electrolytes for sodium rechargeable battery application. Ionics 25:541–549
28. Xu B, Ma X, Tian J, Zhao F, Liu Y, Wang B, Yang H, Xia Y (2019) Layer-structured $NbSe_2$ anode material for sodium-ion and potassium-ion batteries. Ionics 25:4171–4177
29. Ellis BL, Nazar LF (2012) Sodium and sodium-ion energy storage batteries. Curr Opin Solid State Mater Sci 16:168–177
30. Jian Z, Zhao L, Pan H, Hu Y-S, Li H, Chen W, Chen L (2012) Carbon coated $Na_3V_2(PO_4)_3$ as novel electrode material for sodium ion batteries. Electrochem Commun 14:86–89
31. Komaba S, Murata W, Ishikawa T, Yabuuchi N, Ozeki T, Nakayama T, Ogata A, Gotoh K, Fujiwara K (2011) Electrochemical Na insertion and solid electrolyte interphase for hard-carbon electrodes and application to Na-ion batteries. Adv Funct Mater 21:3859–3867
32. Velez V, Ramos-Sánchez G, Lopez B, Lartundo-Rojas L, González I, Sierra L (2019) Synthesis of novel hard mesoporous carbons and their applications as anodes for Li and Na ion batteries. Carbon 147:214–226
33. Xiong Y, Qian J, Cao Y, Ai X, Yang H (2016) Electrospun TiO$_2$/C nanofibers as a high-capacity and cycle-stable anode for sodium-ion batteries. ACS Appl Mater Interfaces 8:16684–16689
34. Xia J, Jiang K, Xie J, Guo S, Liu L, Zhang Y, Nie S, Yuan Y, Yan H, Wang X (2019) Tin disulfide embedded in N-,S-doped carbon nanofibers as anode material for sodium-ion batteries. Chem Eng J 359:1244–1251
35. Yan X, Sun D, Jiang J, Yan W, Jin Y (2017) Self-assembled twine-like $Na_2Ti_3O_7$ nanostructure as advanced anode for sodium-ion batteries. J Alloys Compd 697:208–214
36. Didier C, Guignard M, Denage C, Szajwaj O, Ito S, Saadoune I, Darriet J, Delmas C (2011) Electrochemical Na-deintercalation from $NaVO_2$. Electrochem Solid-State Lett 14:A75–A78
37. Aravindan V, Ling WC, Hartung S, Bucher N, Madhavi S (2014) Carbon-coated $LiTi_2(PO_4)_3$: an ideal insertion host for lithium-ion and sodium-ion batteries. Chem-Asian J 9:878–882
38. Xu C, Xu Y, Tang C, Wei Q, Meng J, Huang L, Zhou L, Zhang G, He L, Mai L (2016) Carbon-coated hierarchical $NaTi_2(PO_4)_3$ mesoporous microflowers with superior sodium storage performance. Nano Energy 28:224–231
39. Kim DJ, Ponraj R, Kannan AG, Lee H-W, Fathi R, Ruffo R, Mari CM, Kim DK (2013) Diffusion behavior of sodium ions in $Na_{0.44}MnO_2$ in aqueous and non-aqueous electrolytes. J Power Sources 244:758–763
40. Berthelot R, Carlier D, Delmas C (2011) Electrochemical investigation of the P2-Na_xCoO_2 phase diagram. Nat Mater 10:74–80
41. Mao J, Luo C, Gao T, Fan X, Wang C (2015) Scalable synthesis of $Na_3V_2(PO_4)_3$/C porous hollow spheres as a cathode for Na-ion batteries. J Mater Chem A 3:10378–10385
42. Zhu Y, Xu Y, Liu Y, Luo C, Wang C (2013) Comparison of electrochemical performances of olivine $NaFePO_4$ in sodium-ion batteries and olivine $LiFePO_4$ in lithium-ion batteries. Nanoscale 5:780–787
43. Wei Z, Wang D, Li M, Gao Y, Wang C, Chen G, Du F (2018) Fabrication of hierarchical potassium titanium phosphate spheroids: a host material for sodium-ion and potassium-ion storage. Adv Energy Mater 8:1801102–1801110
44. Wu XY, Sun MY, Shen YF, Qian JF, Cao YL, Ai XP, Yang HX (2014) Energetic aqueous rechargeable sodium-ion battery based on $Na_2CuFe(CN)_6$-$NaTi_2(PO_4)_3$ intercalation chemistry. ChemSusChem 7:407–411
45. Liang J, Wei Z, Wang C, Ma J (2018) Vacancy-induced sodium-ion storage in N-doped carbon Nanofiber@MoS_2 nanosheet arrays. Electrochim Acta 285:301–308
46. Li X, Zhu X, Liang J, Hou Z, Wang Y, Lin N, Zhu Y, Qian Y (2014) Graphene-supported $NaTi_2(PO_4)_3$ as a high rate anode material for aqueous sodium ion batteries. J Electrochem Soc 161:A1181–A1187
47. Pang G, Yuan C, Nie P, Ding B, Zhu J, Zhang X (2014) Synthesis of NASICON-type structured $NaTi_2(PO_4)_3$-graphene nanocomposite as an anode for aqueous rechargeable Na-ion batteries. Nanoscale 6:6328–6334
48. Li Z, Young D, Xiang K, Carter WC, Chiang Y-M (2013) Towards high power high energy aqueous sodium-ion batteries: the $NaTi_2(PO_4)_3$/$Na_{0.44}MnO_2$ system. Adv Energy Mater 3:290–294
49. Kabbour H, Coillot D, Colmont M, Masquelier C, Mentre O (2011) α-$Na_3M_2(PO_4)_3$ (M=Ti,Fe): absolute cationic ordering in NASICON-type phases. J Am Chem Soc 133:11900–11903
50. Sun M, Han X, Chen S (2018) $NaTi_2(PO_4)_3$@C nanoparticles embedded in 2D sulfur-doped graphene sheets as high-performance anode materials for sodium energy storage. Electrochim Acta 289:131–138
51. Cen C, Chen Z, Xu D, Jiang L, Chen X, Yi Z, Wu P, Li G, Yi Y (2020) High quality factor, high sensitivity metamaterial graphene-perfect absorber based on critical coupling theory and impedance matching, Nanomaterials, 10. https://doi.org/10.3390/nano10010095
52. Zuo Y, Chen L, Zuo Z, Huang Y, Liu X (2017) Rational construction of $NaTi_2(PO_4)_3$@C nanocrystals embedded in graphene sheets as anode materials for Na-ion batteries. Ceram Int 43:12915–12919
53. Aragón MJ, Vidal-Abarca C, Lavela P, Tirado JL (2014) High reversible sodium insertion into iron substituted $Na_{1+x}Ti_{2-x}Fe_x(PO_4)_3$. J Power Sources 252:208–213
54. Wei P, Liu Y, Su Y, Miao L, Huang Y, Liu Y, Qiu Y, Li Y, Zhang X, Xu Y, Sun X, Fang C, Li Q, Han J, Huang Y (2019) F-doped

$NaTi_2(PO_4)_3$/C nanocomposite as a high-performance anode for sodium-ion batteries. ACS Appl Mater Interfaces 11:3116–3124

55. Li X, Wang S, Tang X, Zang R, Li P, Li P, Man Z, Li C, Liu S, Wu Y, Wang G (2019) Porous $Na_3V_2(PO_4)_3$/C nanoplates for high-performance sodium storage. J Colloid Interface Sci 539:168–174
56. Li L, Liu X, Tang L, Liu H, Wang Y-G (2019) Improved electrochemical performance of high voltage cathode $Na_3V_2(PO_4)_2F_3$ for Na-ion batteries through potassium doping. J Alloys Compd 790: 203–211
57. Cao Y, Liu Y, Zhao D, Zhang J, Xia X, Chen T, Zhang L-c, Qin P, Xia Y (2019) K-doped $Na_3Fe_2(PO_4)_3$ cathode materials with high-stable structure for sodium-ion stored energy battery. J Alloys Compd 784:939–946